geoconvention
Calgary • Canada • May 13-17 2019

Enhancing the Structural Fidelity of Magnetotelluric Inversion – An Example from the Bolivian Foothills

Federico Golfré Andreasi[1], Mauro Pezzoli[1], Simone Re[1], Evanz Lazaro[2] and Sergio Burga[2]
[1]Schlumberger, [2]YPFB CHACO SA

Summary

The exploration of the Tarija Basin in South America focuses on the deep Devonian-age Huamampampa and Santa Rosa formations, where hydrocarbon structural traps of hanging wall anticlines formed due to continued thrusting. The sub-Andean fold and thrust belt is primarily a dual system with a major thrust-fault detachment in the deep Kirusillas shale and a second detachment in the younger Los Monos shale formation. Because the shallow structure does not necessarily conform to the deeper structure, it is difficult to predict the geometries of the deeper Devonian traps. Furthermore, the thrusting yields in the Sub-Andean Basin structure, is characterized by steep layers, lateral velocity variations and abrupt topographic changes.
The seismic surveys conducted in this area generally provide seismic records with poor signal-to-noise ratio subsequently resulting in noisy stack sections that are difficult to interpret. Therefore, mapping the thrust anticline core with a satisfactory degree of confidence is a challenging task (Nicanoff et al. 2006) and the economic risk related to a misinterpretation of the structural setting is unacceptable. This risk can be reduced by complementing the exploration program with other geophysical data that do not suffer from the same limitations in terms of illumination and signal-to-noise ratio that affects the seismic data.
The magnetotelluric (MT) method has proven to be a valid ally in complementing the seismic imaging (Tartaras et al. 2011). This is the reason why, a magnetotelluric acquisition and modeling campaign was carried out in the Tarija Basin with the objective of improving the imaging of the Paleozoic section and to map the top of the Huamampampa sandstone reservoir (**Error! Reference source not found.Error! Reference source not found.**).
We present an approach for MT inversion that tries to maximize, simultaneously, the data fit and the structural fidelity by incorporating the available a priori geological information into the inversion process. The advantages deriving from applying this technique for the inversion of the MT soundings acquired in the Tarija Basin are discussed and compared with the more conventional approach presented in Pezzoli et al. (2018) that exploits all the available a priori information for the definition of the starting model.

Inversion methodology

We solve the inverse MT problem by minimizing a cost function through a preconditioned non-linear conjugate gradient technique, as described by Golfré Andreasi and Masnaghetti (2015). The cost function to be minimized by the inversion process can be written as:

$$\Phi(\mathbf{m}) = \Phi_D(\mathbf{m}, d_{obs}) + \Phi_R(\mathbf{m}, \mathbf{m}_{pri})$$

where $\Phi_D(\mathbf{m})$ represents the data misfit term – difference between synthetic and observed data, d_{obs}, weighted by the data covariance – as a function of the model parameter vector to be inferred

($\mathbf{m}$); and $\Phi_R(\mathbf{m})$ is a regularization term that imposes a smoothness constraint over the spatial distribution of the model parameters with respect to the a priori model, $\mathbf{m}_{pri}$. In the conventional inversion scheme the a priori information is inserted and sealed into $\mathbf{m}_{pri}$.
This approach has two main drawbacks: on one side, the choice of the a priori model is heavily biasing the outcome of the inversion of ill-posed problems. On the other side, this approach fixes the knowledge in the a priori model and requests the inversion to move smoothly away from it.
To overcome these limitations, we change the inverse problem formulation by decoupling the a priori information source from the a priori model (Golfré Andreasi et al. 2018). The goal is to dynamically inject the available knowledge on the geological setting into the inverse process without acting on the a priori model. This is achieved by modifying the cost function in the following manner:

$$\Phi(\mathbf{m}) = \Phi_D(\mathbf{m}, d_{obs}) + \Phi_R(\mathbf{m}, \mathbf{m_{pri}}) + \Phi_G(\mathbf{m})$$

where $\boldsymbol{\Phi_G}$ is the term that constrains – in a least-square sense – the spatial distribution of the resistivity to follow some predefined geometry. With the problem formulated in this way, the inversion algorithm tries to find a solution that satisfies the data $\boldsymbol{\Phi_D}$, the generic spatial smoothness constraint $\boldsymbol{\Phi_R}$ and the structural or geological constraint $\boldsymbol{\Phi_G}$.
Golfré Andreasi et al. (2018) propose two different methods for building the Φ_G term starting from a "reference image" that defines the shape of the subsurface structures – an example of reference image is depicted in Figure 2. The first method is based on the definition of an empirical function f that goes from the discrete domain of the regions into the continuous domain of the resistivity thus defining a "reference" resistivity model.

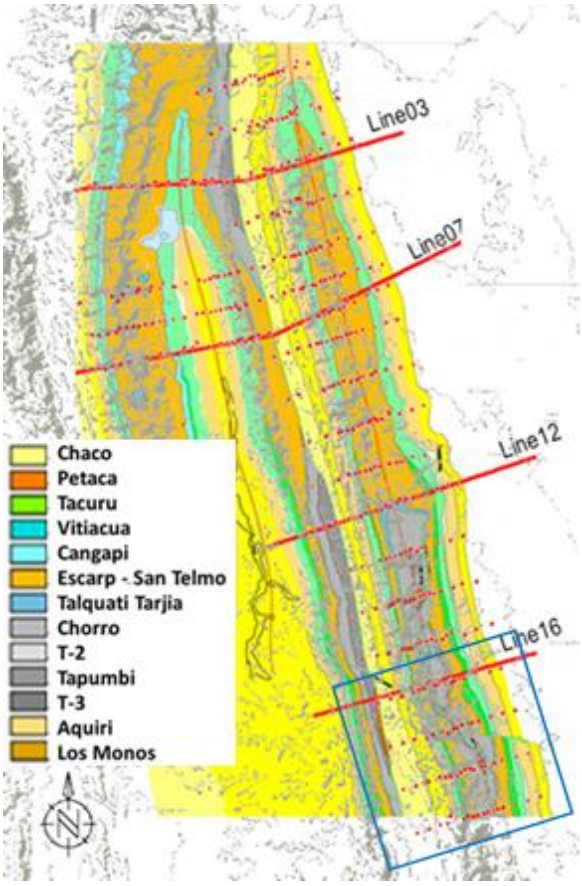

***Figure 1**. Geological map of the MT survey area with gray contour lines indicating the elevation. The red lines are the 2D seismic lines while the red dots represent the MT stations.*

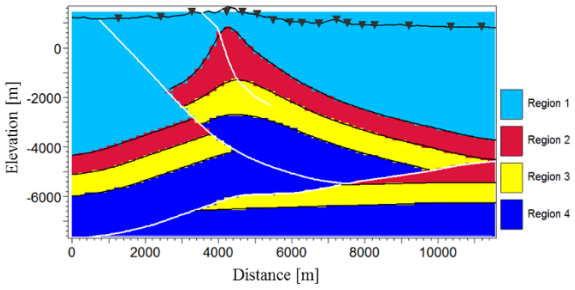

***Figure 2**. Example of a reference image along Line 16. Faults are represented with white lines, while interpretations are represented as black lines. The black triangles represent MT site locations.*

If we indicate with $\Phi_{GE}(\mathbf{m})$ this regularization term we can express it as:

$$\Phi_{GE}(\mathbf{m}) = \lambda|\mathbf{m} - f(\mathbf{k})|^2; \quad f: \mathbb{N} \rightarrow \mathbb{R},$$

where f is the function mentioned above, $\mathbf{k}$ represents the spatial distribution of guiding model and $|\cdot|^2$ indicates the L2-norm of the quantity in the brackets.
The second method relies on the geometrical similarity between the resistivity model and the guiding image and uses the cross-gradient between the resistivity model and the reference image as a measure of the structural similarity (De Stefano et al. 2011; Gallardo and Meju 2007). The corresponding $\Phi_{GX}(\mathbf{m})$ regularization term can be expressed as:

$$\Phi_{GX}(\mathbf{m}) = \lambda|\nabla\mathbf{m} \times \nabla\mathbf{r}|^2.$$

Examples from the Tarija Basin

The two methods discussed above were applied to a set of MT soundings acquired in the Tarija Basin, for YPFB CHACO. The MT survey area covered approximately 800 km^2, surveyed by 400 MT stations along 19 profiles perpendicularly oriented with respect to the local strike of the main anticlinal. The dataset shows, in average, a very good quality, with varying levels of noise typically affecting the high-frequency band and the last decade of frequency (100 s – 1000 s) where the low signal level affects mainly the data due to the minor statistics. The low-frequency dead band (around 1Hz) was generally very well recovered, resulting in smooth sounding curves and good statistics across the required frequency range (1 kHz to 0.001 Hz).
To validate the technique, we carried out 3D inversions that covered approximately 200 km^2 in the area indicated by the blue rectangle shown in Figure 1. In this area, interpreted horizons for the Los Monos and the Huamampampa formations were available. The interpreted horizons were used to define the reference image shown in Figure 2. The same interpretations and one available well log were exploited also for building and calibrating the a priori model (Figure 3a) used in the conventional inversion workflow discussed in Pezzoli et al. (2018). The result of the geologically unconstrained inversion is shown in **Error! Reference source not found.**b.
When using the empirical constraint, the starting model can be uniform, thus removing the initial bias (**Error! Reference source not found.**c). When adopting the cross-gradient approach, instead, the starting model cannot be uniform at this would produce a null gradient along all directions and hence zeroing the cross gradient term. In this case we used the model shown in **Error! Reference source not found.**e which is an intermediate result of an unconstrained inversion workflow. The results of the empirical and cross-gradient inversion are shown, respectively, in **Error! Reference source not found.**d and **Error! Reference source not found.**f.
From a data fit perspective, the three results are equivalent as they reach comparable levels of RMSE (normalized root mean square error) but the constrained solutions show an improved better continuity of the resistivity values within the interpreted layers.
In the shallow portion of the model, just above the anticline, the inversion introduces some resistive structures, regardless the approach adopted. The shallow portion of the model is where the data have the highest sensitivity and it is where the data-driven update prevails over the structural constraint. The presence of a shallow resistive feature is confirmed by the data.

Conclusions

We presented a technique for inverting MT data that embeds in the inverse problem formulation the available a priori geological information. We proposed two possible implementations of the techniques, one based on the use of an empirical function that maps the structural information into a resistivity value and another one that is based on the cross-gradients and brings the structural information in the resistivity model by imposing a geometrical similarity constraint.
The proposed approach removes the bias of including the a priori information in the starting model, hence it is more suited to compare the contribution of different geologic settings in the inversion process with respect to the conventional approach that uses the available a priori information in a static manner as part of the initial model building process.

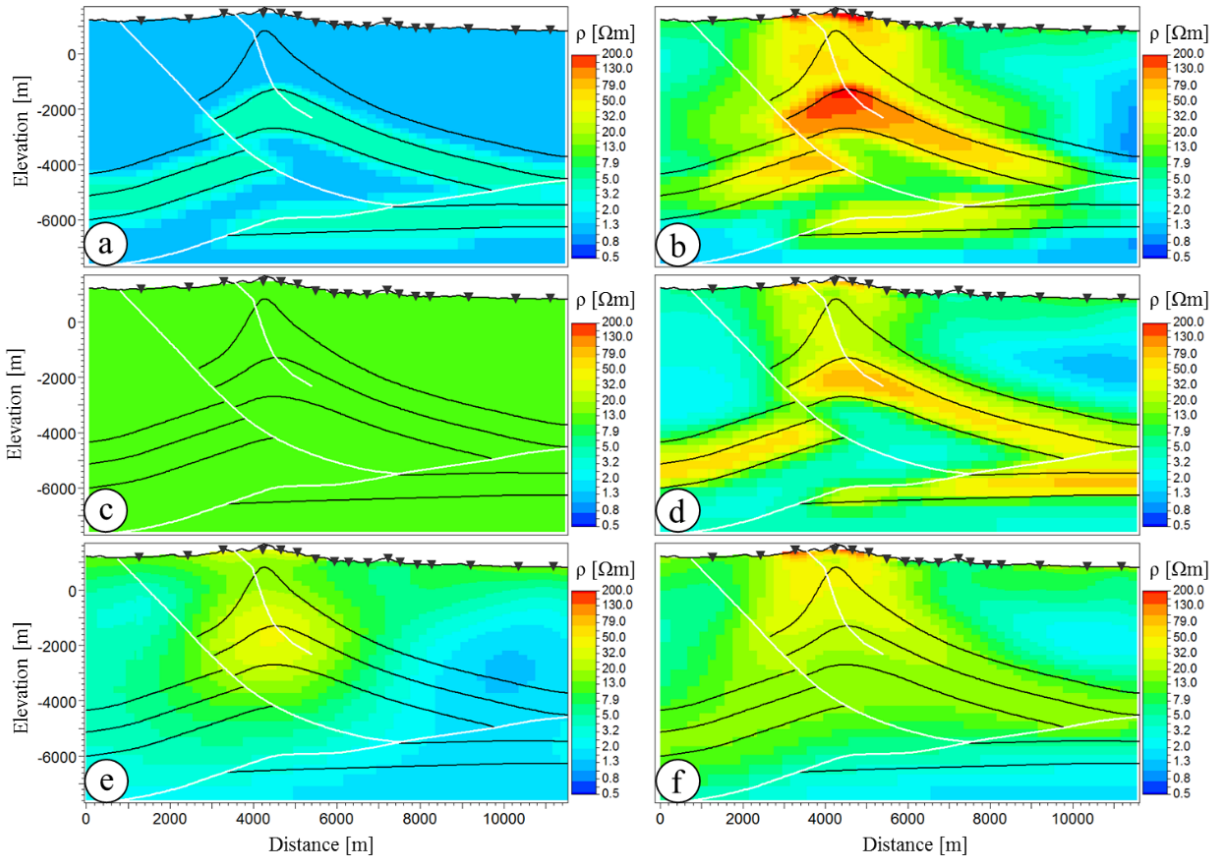

***Figure 3**. Starting (a) and inverted resistivity model (b) of the unconstrained inversion. Starting (c) and inverted (d) model using the empirical structural constraint. Starting (e) and inverted (f) model using the cross-gradient structural constraint.*

Acknowledgements

The authors thank Dr. Eduardo Paz YPFB CHACO S. A. General Manager for permission to publish the magnetotelluric data and results presented herein**.**

References

De Stefano, M., Golfré Andreasi, F., Re, S., Virgilio, M. and Snyder, F. F. [2011] Multiple-domain, simultaneous joint inversion of geophysical data with application to subsalt imaging. *Geophysics*, **76**(3), R69-R80.

Gallardo, L. A. and Meju, M. A. [2007] Joint two-dimensional cross-gradient imaging of magnetotelluric and seismic traveltime data for structural and lithological classification. *Geophysical Journal International*, **169**(3), 1261-1272.

Golfré Andreasi, F. and Masnaghetti, L. [2015] Decoupled Model Grids for Simultaneous Joint Inversion of MT and CSEM Data. *77th EAGE Conference and Exhibition* Extended Abstracts, N105.

Golfré Andreasi, F., Re, S., Ceci, F. Masnaghetti, L. and Battaglini A., [2018] Geologically-Driven Inversion of Magnetotelluric Data. *2nd Conference on Geophysics for Mineral Exploration and Mining*, Extended Abstract

Nicanoff, L., Perez, Y., Yilmaz, O., Dai, N. and Zhang, J. [2006] A case study for imaging complex structures in the Andean thrust belt of Bolivia. *76th Annual International Meeting SEG* Expanded Abstracts, 500-504.

Pezzoli, M., Lazaro, E. And Cuevas, N. [2018] Enhancing Imaging of the Sub-Andean Foothills Geology Using Magnetotelluric. A Case History of a Magnetotelluric Campaign. *80th EAGE Conference and Exhibition* Extended Abstract

Tartaras, E., Masnaghetti, L., Lovatini, A., Hallinan, S., Mantovani, M., Virgilio, M., Soyer, W., De Stefano, M., Snyder, F., Subia, J. And Dugoujard, T. [2011] Multi-property earth model building through data integration for improved subsurface imaging. *First Break*, **29**(4), 83-88.